Materials Transactions, Vol. 61, No. 2 (2020) pp. 361 to 367

Fatigue Property and Cytocompatibility of a Biomedical Co–Cr–Mo Alloy Subjected to a High Pressure Torsion and a Subsequent Short Time Annealing

Peng Chen[1], Huihong Liu[2,*], Mitsuo Niinomi[3,4,5,6], Zenji Horita[7], Hidetoshi Fujii[2] and Takao Hanawa[1]

[1]*Institute of Biomaterials and Bioengineering, Tokyo Medical and Dental University, Tokyo 101-0062, Japan*
[2]*Joining and Welding Research Institute, Osaka University, Osaka 567-0047, Japan*
[3]*Institute for Materials Research, Tohoku University, Sendai 980-5377, Japan*
[4]*Department of Materials Science and Engineering, Faculty of Science and Technology, Meijo University, Nagoya 468-8502, Japan*
[5]*Department of Materials and Manufacturing Science, Graduate School of Engineering, Osaka University, Suita 565-0871, Japan*
[6]*Faculty of Chemistry, Materials and Bioengineering, Kansai University, Osaka 564-860, Japan*
[7]*Department of Materials Science and Engineering, Faculty of Engineering, Kyushu University, Fukuoka 819-0395, Japan*

In the present study, we evaluated the effects of high pressure torsion (HPT) and subsequent short time annealing processing on fatigue properties and cytocompatibility of the biomedical Co–Cr–Mo alloy (CCM). Before processing, CCM was solution treated (CCM_{ST}) to achieve a microstructure composed of coarse single γ-phase equiaxed grains with no internal strain. Through HPT processing, an inhomogeneous microstructure containing both micro- and nano-scaled grains is obtained in CCM specimens, which were named as CCM_{HPT}, accompanied by high internal strain and extensive ε martensite. Following a subsequent short time annealing, a uniform single γ-phase ultrafine-grained microstructure with small local strain fields dispersed forms in CCM specimens, which were named as CCM_{HPTA}. This microstructure change improves fatigue strength in CCM_{HPT}, and further in CCM_{HPTA}, because of the enhanced crack initiation and/or propagation resistance. For cytocompatibility evaluation, the cells cultured on CCM_{ST} show an immobilization tendency, while those cultured on CCM_{HPT} exhibit a locomotion tendency. The cells cultured on CCM_{HPTA} have an intermediate pattern. Compared with CCM_{ST}, much larger numbers of cells are proliferated in both CCM_{HPT} and CCM_{HPTA}. All these results demonstrate that the CCM_{HPTA} offers an improved fatigue property and a good cytocompatibility. Therefore, it is promising for use in biomedical applications. [doi:10.2320/matertrans.MT-M2019148]

(Received May 27, 2019; Accepted November 6, 2019; Published December 13, 2019)

Keywords: *Co–Cr–Mo alloy, high pressure torsion, annealing, fatigue property, cytocompatibility*

1. Introduction

Because Co–Cr–Mo alloys exhibit good mechanical properties, great biocompatibility, as well as excellent wear resistance, they have been commercially applied as implant materials in abundant biomedical applications such as artificial dental wires and hip and knee joints.[1–3] However, mechanical failure still occurs sometimes in the practical uses of the Co–Cr–Mo alloys, and the wear debris of these alloys, which induce metallosis, might lead to an allergy issue.[4] Therefore, it is required to further enhance the mechanical properties of the Co–Cr–Mo alloys to reduce their wear and failure risks. This improvement will benefit biomedical applications.

High pressure torsion (HPT) is one of the severe plastic deformation (SPD) methods, in which a high pressure and a large torsional straining are applied on a disk specimen so that the extremely high dislocation density and extremely large strain can be introduced into the material to facilitate significant grain refinement and/or phase transformations.[5–11] In a previous study,[12] HPT processing was adopted into a Co–Cr–Mo alloy, Co–28Cr–6Mo (mass%, hereafter abbreviated as CCM), at a rotation number of 0.25, a rotation speed of 1 rpm, and a high pressure of 6 GPa, to improve the mechanical properties by introducing significant grain refinement into nano-scale and extensive γ (face-centered cubic, FCC) to ε (hexagonal closed-packed, HCP) martensitic transformation. The mechanical strength of the CCM alloy was indeed significantly improved via nano-scaled grain refinement, large internal strain associated with high dislocation density, and hard ε martensitic transformation. However, all of these inevitably deteriorate the ductility of the CCM alloy because they play a strong effect on impeding the dislocation gliding and dislocation multiplication. In addition, the transformed ε martensite with an HCP structure having limited slip systems shows poor ductility which also contributes to the reduced ductility of the CCM alloy.[12] A short time annealing was carried out on this HPT processed CCM alloy (CCM_{HPT}) to improve the ductility of the CCM_{HPT} alloy while maintaining its high mechanical strength by properly removing the excessive hard ε martensite and releasing the large internal strain while maintaining the ultrafine-grained microstructure.[13] The CCM_{HPT} alloy subjected to the short time annealing at 1273 K for a duration of 0.3 ks (CCM_{HPTA}) indeed exhibits a recovered elongation of ~12% with a maintained high tensile strength of ~1600 MPa compared with the CCM_{HPT} alloy (elongation: ~1%, tensile strength: ~1700 MPa) and the solution treated CCM alloy (CCM_{ST}, elongation: ~15%, tensile strength: ~1000 MPa) as illustrated in Fig. 1.[13] However, the fatigue properties and cytocompatibility, both of which are extremely crucial properties for the CCM_{HPTA} alloy to be practically used in biological applications, have still not been investigated in detail. In this study, the fatigue properties and cytocompatibility of the CCM_{ST}, CCM_{HPT}, as well as CCM_{HPTA} alloys were comparatively investigated to evaluate the applicability of the CCM_{HPTA} alloy in biological uses. The relationship between processing conditions, including HPT and short time annealing, microstructure, and properties including fatigue properties and cytocompatibility of the CCM alloy was discussed.

*Corresponding author, E-mail: liuhh@jwri.osaka-u.ac.jp

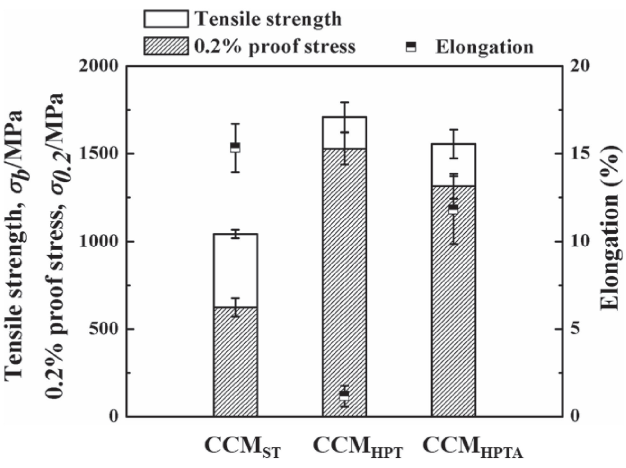

Fig. 1 Tensile properties of CCM_{ST}, CCM_{HPT}, and CCM_{HPTA}.[13)]

2. Experimental Procedures

2.1 Materials preparation

A hot-forged CCM alloy rod having a diameter of 25 mm was applied in the present study. The chemical composition of the alloy is the same with that shown in the previous study.[13)] The hot-forged CCM rod was firstly subjected to a solution treatment at 1473 K for a duration of ~3.6 ks in vacuum (CCM_{ST}). The obtained CCM_{ST} rod was then cut into disk-shaped specimens with the diameter of 10 mm and the thickness of 1 mm. A HPT processing was conducted on the CCM_{ST} disk-shaped specimens under a quasi-constrained condition at a rotation number of 0.25, a rotation speed of 1 rpm, and a high pressure of 6 GPa at room temperature (CCM_{HPT}). The CCM_{HPT} specimens were subsequently subjected to a short time annealing at 1273 K for a duration of 0.3 ks in vacuum (CCM_{HPTA}).

2.2 Microstructural analysis

The microstructure of the CCM_{ST}, CCM_{HPT}, and CCM_{HPTA} specimens was investigated using an electron backscatter diffraction (EBSD) at the designated position as schematically illustrated in Fig. 2(a). The specimens were subjected to a mechanical polishing using the SiC waterproof emery papers up to 2400 grits, and then a mirror polishing using the colloidal SiO_2 suspension.

2.3 Fatigue property evaluation

The fatigue specimens with dimensions based on the standard (ASTM E466) were prepared from the CCM_{ST}, CCM_{HPT}, and CCM_{HPTA} specimens, as schematically illustrated in Fig. 2(b). The specimen surfaces were mechanically polished using the SiC waterproof emery papers, then buff polished to a mirror finishing using the colloidal SiO_2 suspension. The mirror-polished specimens were subsequently subjected to the fatigue tests with a frequency of 10 Hz and a stress ratio of 0.1, under the tension-tension mode at room temperature using an electro-servo-machine. In this study, the fatigue limit was defined as the maximum cyclic stress, at which the specimen still not fatigue fractured under 10^7 cycles. After fatigue failure, the fracture surface morphologies of the specimens were inspected by a scanning electron microscope (SEM). Additionally, the specimens before and after fatigue tests were subjected to an X-ray diffraction (XRD) analysis to quantitatively clarify the volume fraction of the ε martensite in CCM specimens.

2.4 Cytocompatibility evaluation

2.4.1 Cell culture

A mouse preosteoblast cell (MC3T3-E1), was purchased from RIKEN BioResource Center and used directly as described previously.[14)] Briefly, cells were maintained in an alpha modified Eagle's minimum essential medium (α-MEM; Gibco, Carlsbad, CA) supplemented with 10% fetal bovine serum (Gibco) and an antibiotic/antimycotic (Gibco). Before cell seeding, all CCM specimens were immersed in deionized water over 1 week to form a stable oxide surface layer. Then 70% ethanol was used to sterilize all specimens for 20 min and rinsed thoroughly with deionized water, following which cells were seeded onto the specimens with seeding density of 6000 cells$\cdot$cm^{-2}. Cells were cultured at 37°C in a humidified atmosphere of 5% CO_2 in air.

2.4.2 Attached cell counts

According to manufacturer instructions, the attached cell number on each specimen was counted using Cell Counting

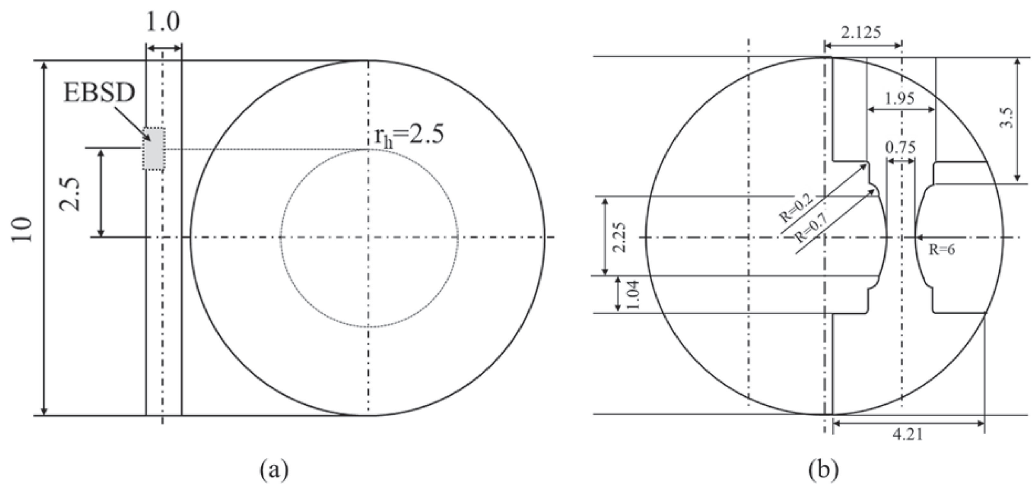

Fig. 2 Schematic illustrations of specimen preparations for (a) EBSD analysis and (b) fatigue tests.

Kit-8 (Dojindo Laboratories, Kumamoto, Japan), which also described elsewhere.[15] Because the cell number and absorbance at 450 nm showed a linear relationship, the attached cell number was calculated based on a prepared standard curve.

2.4.3 Fluorescent staining and imaging

The morphologies of cells on each specimen were visualized by immunofluorescence staining after 6 h incubation, as described in our previous report.[16] Briefly, cells were fixed and blocked before staining. Cellular F-actin was stained with rhodamine phalloidin (Cytoskeleton Inc., Denver, CO), and nuclei were counterstained with 4′,6-diamidino-2-phenylindole (DAPI, Invitrogen, Carlsbad, CA). Adhesion plaques were stained with labeling of vinculin using a monoclonal anti-vinculin antibody (Sigma-Aldrich) and then conjugated with Alexa Fluor 488-conjugated goat anti-mouse IgG (Invitrogen). IX71 microscope with DP70 charge-coupled device camera (Olympus, Tokyo, Japan) was used to acquire digital images.

2.4.4 Statistical analysis

The results of cell proliferation were repeated three independent times ($n \geqslant 3$) and analyzed by ANOVA followed by a S-N-K test using SPSS. A value of p value <0.05 was considered statistically significant.

3. Results and Discussion

3.1 Microstructure

Figure 3 shows the EBSD micrographs of the CCM_{ST}, CCM_{HPT}, and CCM_{HPTA} specimens. The CCM_{ST} specimen[13] shows a microstructure composed of single γ-phase (FCC) equiaxed grains having an average grain diameter of $\sim$70 µm. Annealing twins are extensively identified in the interior of the grains in the CCM_{ST} specimen, which is owing to the low stacking fault energy. The corresponding kernel average misorientation (KAM) map shows that almost no internal strain is detected in the CCM_{ST} specimen, which is because of the stress-released solution treatment. After HPT, deformation-induced γ to ε (HCP) martensitic transformation extensively occurred in the CCM_{HPT} specimen. A large number of black areas, where the crystallographic information is unable to be identified by EBSD because of the existence of nanoscale-grained microstructure and/or the high internal strain, are observed in the CCM_{HPT} specimen. These results suggest that an inhomogeneous microstructure containing both micro-scaled grains and nano-scaled grains formed in the CCM_{HPT} specimen. The KAM map indicates that the CCM_{HPT} specimen shows high internal strain induced by severe plastic deformation throughout the entire specimen. When subjecting the CCM_{HPT} specimen to a short time annealing, the excessive ε martensite was mostly removed, and a uniform single γ-phase ultrafine-grained microstructure having an average grain diameter of $\sim$6.5 µm formed in the CCM_{HPTA} specimen. The KAM map reveals that the internal strain in the CCM_{HPTA} specimen was released significantly compared with that in the CCM_{HPT} specimen, but still leaves small local strain fields dispersed throughout the CCM_{HPTA} specimen. These results match well with those reported in previous works.[11–13]

Figure 4 shows the S-N curves of the CCM_{ST}, CCM_{HPT}, and CCM_{HPTA} specimens, in which the maximum cyclic stress are plotted as a function of the number of cycles to failure. The CCM_{ST} specimen shows the lowest fatigue strength, and the lowest fatigue limit of $\sim$400 MPa among the examined specimens. After HPT, the CCM_{HPT} specimen exhibits higher fatigue strength compared to the CCM_{ST}

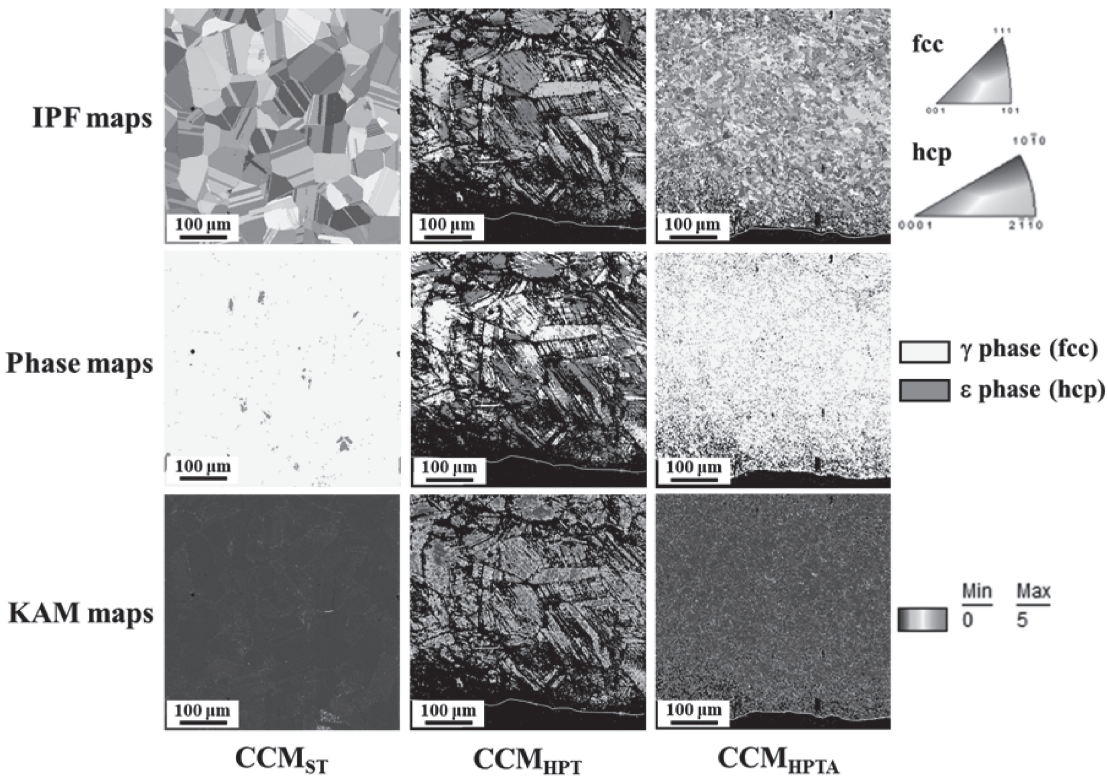

Fig. 3 EBSD results of CCM_{ST},[13] CCM_{HPT}, and CCM_{HPTA}.

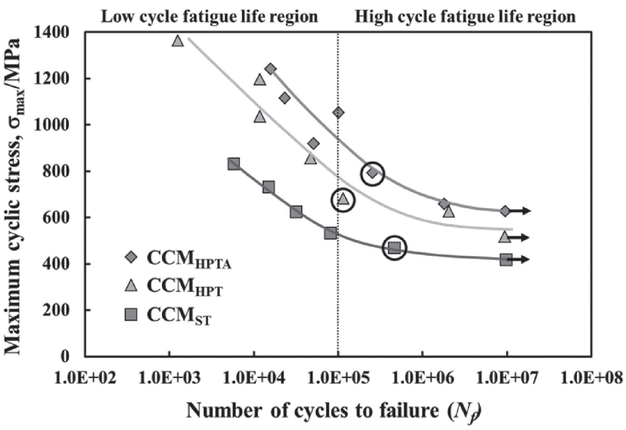

Fig. 4 S-N curves of CCM_{ST}, CCM_{HPT}, and CCM_{HPTA}.

specimen in both low-cycle fatigue-life region where failure occurs below 10^5 cycles, and high-cycle fatigue-life region, in which the number of cycles to failure exceeds 10^5 cycles; the fatigue limit of the CCM_{HPT} specimen is thus improved to ~520 MPa. When the short time annealing was conducted following HPT processing, the fatigue strength is further improved in the CCM_{HPTA} specimen in both low-cycle and high-cycle fatigue-life region compared to that of the CCM_{HPT} specimen; the CCM_{HPTA} specimen shows the highest fatigue limit of ~630 MPa among the examined specimens.

3.2 Fatigue properties

The fatigue fractographs of the CCM_{ST}, CCM_{HPT}, and CCM_{HPTA} specimens fractured in the high-cycle fatigue-life region were inspected by SEM (the fractured specimens chosen for observations are marked by circles in Fig. 4); the corresponding results are demonstrated in Fig. 5. Because the fatigue fractographs of the specimens fractured in the low-cycle fatigue-life region show similar morphologies to those of the specimens fractured in the high-cycle fatigue-life region, only the results of the latter are exhibited in the present study. In the CCM_{ST} specimen, two crack initiation sites, indicated by the red arrows in Fig. 5(a), are identified near the specimen surface, which suggests that the fatigue cracks initiated on the specimen surface in the CCM_{ST} specimen during fatigue tests. Facets with a facet width of ~25 µm are identified in the fatigue crack propagation area in the CCM_{ST} specimen, as marked by the rectangle in Fig. 5(b). Furthermore, the striations can be clearly observed on the observed facets, as shown in Fig. 5(c). In the CCM_{HPT} specimen, several crack initiation sites are identified near the specimen surface, as pointed out by the red arrows in Fig. 5(d). Facets are also detected in the fatigue crack propagation area in the CCM_{HPT} specimen, as marked by the rectangle in Fig. 5(e), whereas the width of the facets observed in the CCM_{HPT} specimen is smaller than that in the CCM_{ST} specimen. Moreover, the striations are also visible in the CCM_{HPT} specimen, as shown in Fig. 5(f). It is thus known that both of the CCM_{ST} and CCM_{HPT} specimens show facet and striation morphologies in the fatigue fracture surfaces, whereas the CCM_{HPTA} specimen exhibits a completely different fatigue fracture morphology. In the CCM_{HPTA} specimen, only one crack initiation site is observed on the specimen surface, as indicated by the red arrow in Fig. 5(g). In the fatigue crack propagation area, neither facets nor striations, but only small dimples are observed in the CCM_{HPTA} specimen, as shown in Figs. 5(h) and 5(i).

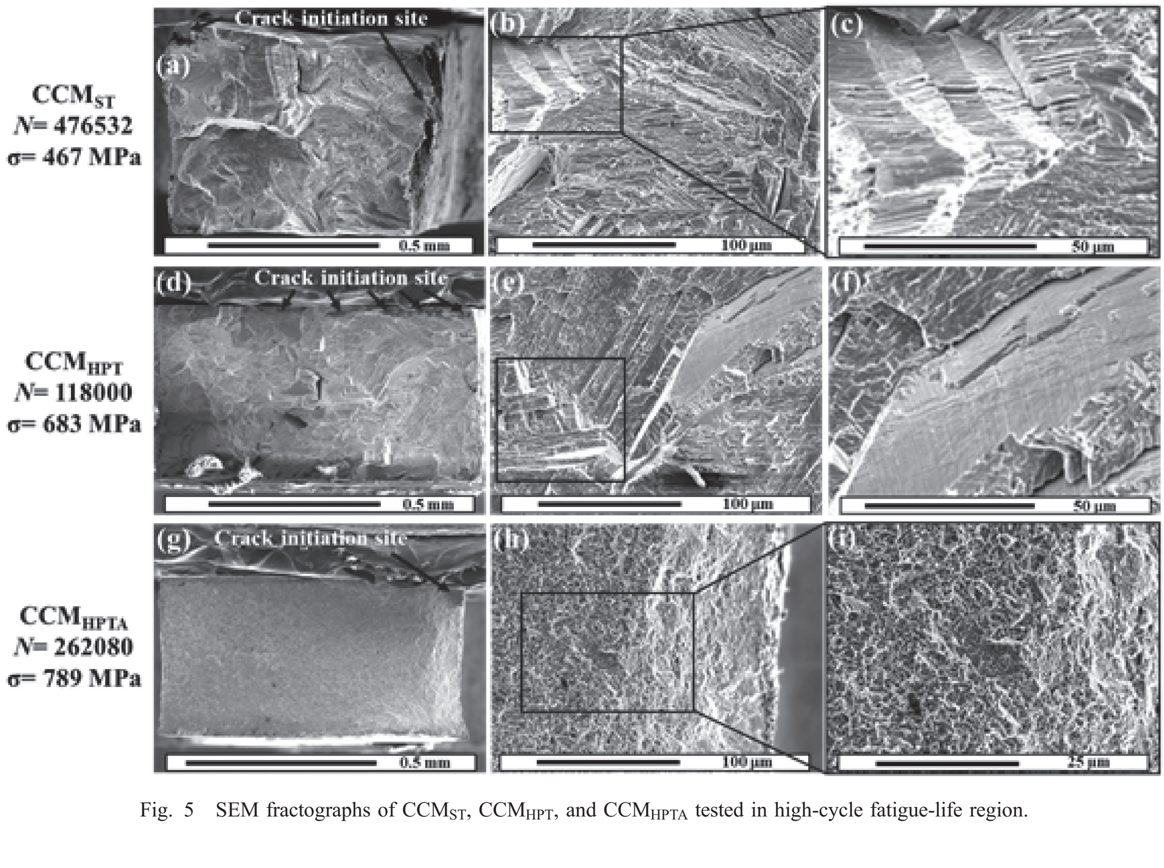

Fig. 5 SEM fractographs of CCM_{ST}, CCM_{HPT}, and CCM_{HPTA} tested in high-cycle fatigue-life region.

As shown by the above results, the fatigue cracks initiated on the specimen surfaces in all the three investigated specimens. The CCM_{HPTA} specimen shows the highest crack initiation resistance because it shows the least crack initiation sites even though it is under the highest cyclic stress. According to Fig. 3, the CCM_{ST} specimen shows a microstructure consisting of coarse single-γ-phase equiaxed grains with no internal strain, while the CCM_{HPT} specimen has an inhomogeneous microstructure composed of micro-scaled γ grains, ε martensite and local areas containing nano-scaled grains, and/or extremely high internal strain. The increased number of crack initiation sites in the CCM_{HPT} specimen compared to the CCM_{ST} specimen is thus considered to be attributed to the applied high cyclic stress and/or the inhomogeneous microstructure in which the stress concentration can easily occur in the border of the hard brittle regions and soft ductile regions, thus causing crack initiations. In addition, the CCM_{HPTA} specimen shows a uniform single γ-phase ultrafine-grained microstructure with small local strain fields uniformly distributed. This homogeneous ultrafine microstructure effectively disperses the stress uniformly throughout the entire specimen and reduces the risk of the occurrence of stress concentration, thereby improving the crack initiation resistance in the CCM_{HPTA} specimen.

In the fatigue crack propagation area, facets and striations can be observed in both the CCM_{ST} and CCM_{HPT} specimens. It is likely that the facets formed because the fracture occurred along the phase boundaries between γ phases and ε martensite lamellar. Table 1 lists the calculated volume fraction of the ε martensite in the CCM_{ST}, CCM_{HPT}, and CCM_{HPTA} specimens before and after high cycle fatigue tests based on the XRD analysis (The calculation procedure is the same as that reported in previous works[11] and not shown here). After fatigue tests, it is observed that the volume fraction of the ε martensite significantly increased from 0% to 49% in the CCM_{ST} specimen. However, no obvious variation in ε martensite volume fraction can be identified in either the CCM_{HPT} specimen (from 87% to 89%), which is because of the large volume fraction of ε martensite originally formed before fatigue tests, or the CCM_{HPTA} specimen (from 2% to 5%), which is considered to be attributed to the ultrafine-grained microstructure that may stabilize the γ phase and increase the resistance for γ to ε martensitic transformation.[17,18] These results reveal that the stress-induced martensitic transformation occurred in the CCM_{ST} specimen during fatigue cyclic loading, which explains the facet formation in the fracture surface of the CCM_{ST} specimen. The volume fraction of the ε martensite is much larger in the CCM_{HPT} specimen compared to that in the CCM_{ST} specimen, even after fatigue tests. Therefore, the more martensite lamellar in the CCM_{HPT} specimen provides more barriers and more complicated paths for fatigue cracks to propagate, thereby enhancing the fatigue crack propagation resistance in the CCM_{HPT} specimen. In the CCM_{HPTA} specimen, because almost no ε martensite formed before or after fatigue tests, no facet can be identified in the fracture surface. The dimple-type fracture morphology suggests that the uniform ultrafine-grained microstructure with uniformly distributed small local strain fields in the CCM_{HPTA} specimen seems to provide a high resistance for the fatigue crack propagation because stress is difficult to concentrate within this microstructure.

3.3 Cytocompatibility

Cell adhesions on the CCM_{ST}, CCM_{HPT}, and CCM_{HPTA} specimens were visualized by immunofluorescence staining after 6 h incubation; the results are shown in Fig. 6. Spreading shapes showed with cytoskeleton staining are similar for all CCM specimens. Although it has been reported that HPT processed Ti alloy (TNTZ) promoted cell adhesion and migration by visualization of actin filaments,[19] in this study, the interactions between cells and CCM substrates were detected by visualization of adhesion plaques through vinculin staining.[20–22] Interestingly, for adhesion plaques vinculin, depending on the processing, differences in the distribution and shape were detected. Cells cultured on CCM_{ST} specimen and CCM_{HPTA} specimen present a fibrous structure at the margin of the pseudopodia, compared with those cultured on the CCM_{HPT} specimen. By contrast, cells growing on the CCM_{HPT} specimen and the CCM_{HPTA} specimen display a pointed distribution of adhesion plaques in cells. As known the role of vinculin during cell adhesion behavior,[20,21] the shapes of cells cultured on the CCM_{HPT} specimen indicate a stronger cell locomotion trend, on the other hand, those on the CCM_{ST} specimen present a stronger immobilization trend. Cells cultured on the CCM_{HPTA} specimen show an intermediate pattern. As reported previously that nano-scaled grains ($\sim$100 nm) promoted cellular locomotion,[20] cells cultured on the CCM_{HPT} specimen show a locomotion trend compared with those cultured on CCM specimens with micro-scaled grains, where CCM_{ST} exhibits an average grain diameter of $\sim$70 µm, and CCM_{HPTA} has an average grain diameter of $\sim$6.5 µm (Fig. 3). However, the different cellular adhesion behaviors of the CCM_{ST} and CCM_{HPTA} specimens were detected, which indicates that the uniformly distributed small local strain fields or newly formed grain boundaries in CCM_{HPTA} could have an effect on the promotion of cell locomotion.

Table 1 Volume fractions of ε phase in CCM_{ST}, CCM_{HPT}, and CCM_{HPTA} before fatigue tests and after high cycle fatigue tests based on XRD analyses.

	Before fatigue tests	**After fatigue tests**
CCM_{ST}	0%	49%
CCM_{HPT}	87%	89%
CCM_{HPTA}	2%	5%

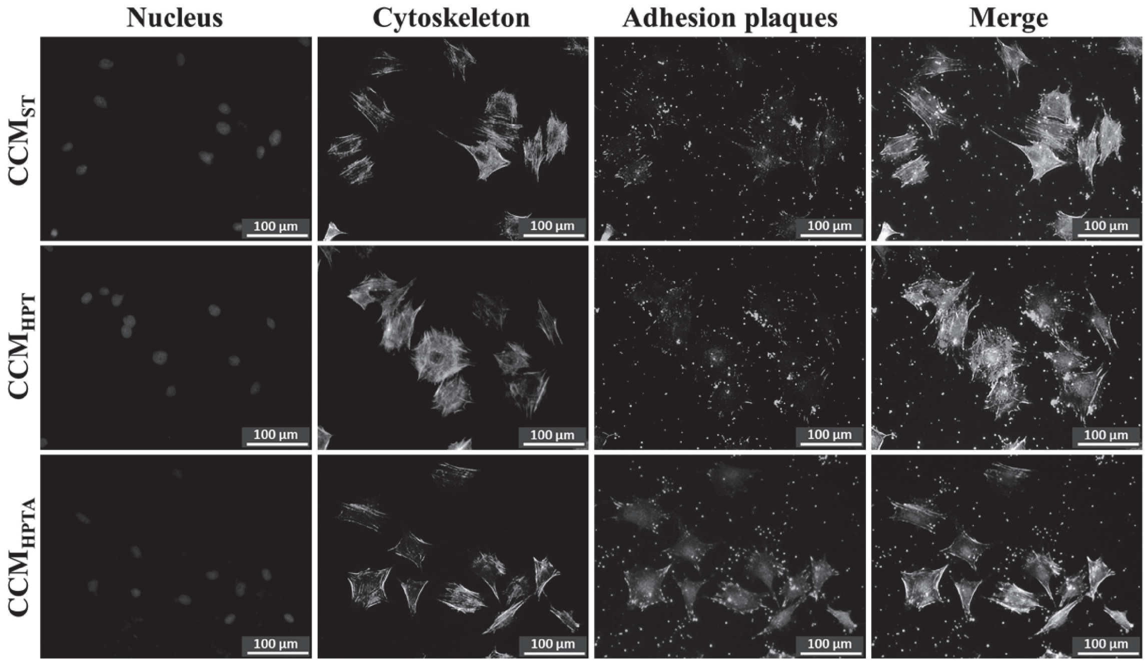

Fig. 6 Initial cellular morphologies of MC3T3-E1 attached to CCM_{ST}, CCM_{HPT}, and CCM_{HPTA} after a 6-h incubation. With a fluorescent staining, cellular nuclei, F-actin, and vinculin were visualized with blue, red, and green, respectively.

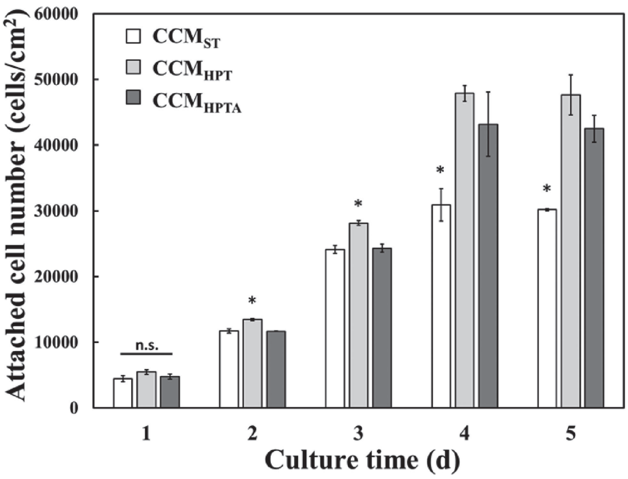

Fig. 7 Cellular proliferation of MC3T3-E1 cultured on CCM_{ST}, CCM_{HPT}, and CCM_{HPTA}. The "*" represents statistically significant, and the "n.s." represents non-significance.

Cell proliferation was evaluated with all CCM specimens for 5 days, as shown in Fig. 7. With the increasing incubation time, the cell numbers increase for all specimens. No significant difference was observed in cell attachment number among all the examined CCM specimens, after 1-d culture. However, more cells were harvested by the CCM_{HPT} specimen than those by the CCM_{ST} or CCM_{HPTA} specimens were on the second and third days. After 4 to 5 days' culture, a significantly lower number of cells are observed on the CCM_{ST} specimen compared with those on both the CCM_{HPT} and CCM_{HPTA} specimens. These results indicate that compared with CCM with a larger grain diameter (CCM_{ST}), the CCM with a smaller grain diameter corresponding to more newly formed grain boundaries and higher internal strain, which relates to more generated defects such as dislocations (CCM_{HPT} and CCM_{HPTA}), are beneficial to cell proliferation. In addition, it is worth noting that, compared with the CCM_{HPTA} specimen, the CCM_{HPT} specimen with nano-scaled grains, significantly higher internal strain, and extensive ε martensite lamellar showed faster cell growth at the initial cultivation (2∼3 days).

4. Conclusions

Herein, effects of HPT and subsequent short time annealing processing on fatigue properties and cytocompatibility of the CCM alloy were investigated. Before processing, CCM specimens were solution treated (CCM_{ST}) to achieve a microstructure composed of coarse single γ-phase equiaxed grains. After HPT, CCM_{HPT} shows an inhomogeneous microstructure containing both micro- and nano-scaled grains, high internal strain, and extensive ε martensite; by contrast, a uniform single γ-phase ultrafine-grained microstructure with dispersed small local strain fields forms after a subsequent short time annealing in CCM_{HPTA}. This microstructure change improves fatigue strength in CCM_{HPT} and further in CCM_{HPTA} because of the enhanced crack initiation and/or propagation resistance. For cell adhesion behavior, a locomotion trend and an immobilization trend are presented by cells cultured on CCM_{HPT} and cells cultured on CCM_{ST}, respectively. The cells on CCM_{HPTA} show an intermediate pattern. For cell proliferation behavior, after 4 days culture, a similar much larger number of cells are harvested by both CCM_{HPT} and CCM_{HPTA} in comparison with that harvested by CCM_{ST}. Our results indicate that the CCM with an HPT processing followed by a short time annealing (CCM_{HPTA}) shows an improved fatigue property and a good cytocompatibility, which could be a promising material applied for biomedical using.

Acknowledgment

This work was supported by Creation of Life Innovation Materials for Interdisciplinary and International Researcher Development (iLIM) from the Ministry of Education, Culture, Sports, Science and Technology (MEXT), Japan.

REFERENCES

1) S.H. Sun, Y. Koizumi, S. Kurosu, Y.P. Li, H. Matsumoto and A. Chiba: Acta Mater. **64** (2014) 154–168.
2) K. Yamanaka, M. Mori and A. Chiba: Acta Biomater. **9** (2013) 6259–6267.
3) A. Chiba, K. Kumagai, N. Nomura and S. Miyakawa: Acta Mater. **55** (2007) 1309–1318.
4) Y. Koizumi, S. Suzuki, K. Yamanaka, B.S. Lee, K. Sato, Y. Li, S. Kurosu, H. Matsumoto and A. Chiba: Acta Mater. **61** (2013) 1648–1661.
5) A.P. Zhilyaev and T.G. Langdon: Prog. Mater. Sci. **53** (2008) 893–979.
6) H. Yilmazer, M. Niinomi, K. Cho, M. Nakai, J. Hieda, S. Sato and Y. Todaka: Acta Mater. **80** (2014) 172–182.
7) R.B. Figueiredo and T.G. Langdon: Mater. Sci. Eng. A **528** (2011) 4500–4506.
8) S. Scheriau, Z. Zhang, S. Kleber and R. Pippan: Mater. Sci. Eng. A **528** (2011) 2776–2786.
9) M. Kawasaki, B. Ahn and T.G. Langdon: Acta Mater. **58** (2010) 919–930.
10) Y. Ito and Z. Horita: Mater. Sci. Eng. A **503** (2009) 32–36.
11) M. Isik, M. Niinomi, H.H. Liu, K. Cho, M. Nakai, Z. Horita, S. Sato, T. Narushima, H. Yilmazer and M. Nagasako: Mater. Trans. **57** (2016) 1109–1118.
12) M. Isik, M. Niinomi, K. Cho, M. Nakai, H.H. Liu, H. Yilmazer, Z. Horita, S. Sato and T. Narushima: J. Mech. Behav. Biomed. Mater. **59** (2016) 226–235.
13) M. Isik, M. Niinomi, H.H. Liu, K. Cho, M. Nakai, Z. Horita, T. Narushima and K. Ueda: Mater. Trans. **57** (2016) 1887–1896.
14) P. Chen, A. Nagai, Y. Tsutsumi, M. Ashida, H. Doi and T. Hanawa: J. Biomed. Mater. Res. A **104** (2016) 639–651.
15) P. Chen, M. Miyake, M. Tsukamoto, Y. Tsutsumi and T. Hanawa: J. Biomed. Mater. Res. A **105** (2017) 3456–3464.
16) P. Chen, T. Aso, R. Sasaki, M. Ashida, Y. Tsutsumi, H. Doi and T. Hanawa: J. Biomed. Mater. Res. A **106** (2018) 2735–2743.
17) E.A. Owen and D.M. Jones: Proc. Phys. Soc. B **67** (1954) 456–466.
18) J.Y. Huang, Y.K. Wu, H.Q. Ye and K. Lu: Nanostruct. Mater. **6** (1995) 723–726.
19) H. Yilmazer, M. Sen, M. Niinomi, M. Nakai, H.H. Liu, K. Cho, Y. Todaka, H. Shiku and T. Matsue: RSC Advances **6** (2016) 7426–7430.
20) P. Chen, M. Ashida, H. Doi, Y. Tsutsumi, Z. Horita and T. Hanawa: Mater. Trans. **57** (2016) 2020–2025.
21) P. Chen, T. Aso, R. Sasaki, Y. Tsutsumi, M. Ashida, H. Doi and T. Hanawa: J. Biomed. Nanotechnol. **13** (2017) 324–336.
22) J.L. Coll, A. Ben-Ze'ev, R.M. Ezzell, J.L. Rodríguez Fernández, H. Baribault, R.G. Oshima and E.D. Adamson: Proc. Natl. Acad. Sci. USA **92** (1995) 9161–9165.